Green Chemistry

PAPER

View Article Online
View Journal | View Issue

Cite this: *Green Chem.*, 2020, **22**, 8614

A rhenium catalyst with bifunctional pyrene groups boosts natural light-driven CO_2 reduction†

Li-Qi Qiu,‡ Kai-Hong Chen, ‡ Zhi-Wen Yang and Liang-Nian He *

Received 13th September 2020,
Accepted 17th November 2020

DOI: 10.1039/d0gc03111a

rsc.li/greenchem

Developing effective sunlight-driven systems for CO_2 reduction is one of the most promising subjects from the perspective of sustainably producing solar fuels. Herein, we develop a strategy to boost CO_2 reduction performance by enhancing intermolecular electron transfer efficiency and visible light-absorption ability by introducing bifunctional pyrene groups on the ligand. This catalyst exhibits high-efficiency performance for natural light-powered CO_2 reduction (TON_{CO} up to 350 ± 36, Φ_{CO} up to 46.6 ± 3%). This is the first report on using a single-molecule photocatalyst for CO_2 reduction under natural conditions. Through the combination of experimental results and DFT calculations, the appending pyrene groups have been proven to promote the catalyst's ability to harness visible light as well as facilitate electron transfer (ET) through intermolecular π–π interactions. Due to the accelerated intermolecular ET, TON_{CO} can be further boosted up to 1367 ± 32 in the presence of the ruthenium photosensitizer. Moreover, an enhancement in CO_2 electroreduction performance can also be observed for the pyrenyl-functionalized rhenium catalyst further highlighting the versatile applications of this methodology.

Introduction

Controlling the total amount of carbon dioxide (CO_2) in the atmosphere and responding to global warming and energy crisis positively is a critical research topic for scientists.[1,2] Therefore, the conversion of CO_2 into value-added carbon products or fuels has been a significant research field.[3–9] The thermodynamic stability and kinetic inertness of CO_2 make it necessary to overcome a high activation barrier and energy-intensive limitation for performing CO_2 conversion.[10,11] Converting CO_2 into carbon monoxide (CO) using solar energy is an ideal and sustainable way to reduce the concentration of CO_2 in the atmosphere while enabling the solar energy-to-fuel conversion schemes, because CO is an important raw material in the industrial syntheses based on Fischer–Tropsch chemistry.[12] However, the intermittency of solar energy from variable atmospheric conditions is one of the major challenges that make the large scale application of this technology difficult.[13–15] In this context, almost all of the photochemical CO_2 reduction reactions (CO_2RR) were conducted under simulated sunlight sources instead of the sun.[16] No report is available for CO_2RR directly promoted by the sun in homogeneous systems, presumably due to the great challenge for simultaneously overcoming both limitations associated with the visible-light absorption ability and, especially, intermolecular electron transfer (ET) efficiency.

As a widespread event in nature, ET between molecules plays a key role not only in biology but in semiconductors, catalysts, and photoactive materials.[17–21] A persisting fundamental challenge in the design of material with high intermolecular ET efficiency is that the intermolecular ET is sensitive to the material concentration because the non-covalent interactions can form only in a relatively high concentration.[22–24] In the field of CO_2RR, CO_2 is reduced using metal complexes[25–30] through ET from the photosensitizer (PS) to the catalyst (Cat) to drive the reaction (Scheme 1A). Clearly, enhancing ET will be a powerful strategy to design an efficient and selective catalyst for CO_2RR. Accordingly, the Ishitani group developed a series of efficient supramolecular catalysts with short bridging linkers to connect different PS and rhenium (Re) catalysts.[31–34] Because of the acceleration of intramolecular ET between PS and Cat, such supramolecular catalysts exhibit impressive performance in CO_2RR. More recently, an elegant bimolecular system has been reported by Kubiak and coworkers, who utilized hydrogen-bonding interactions between ruthenium (Ru) PS and Re Cat to facilitate intermolecular ET (Scheme 1C), thereby enhancing CO_2RR activity.[35] However, most of these systems suffer from multiple synthetic steps and additional cost of PS. Although a single-molecular catalyst (Scheme 1B) can avoid these problems, pre-

State Key Laboratory and Institute of Elemento-Organic Chemistry, College of Chemistry, Nankai University, Tianjin 300071, P. R. China.
E-mail: heln@nankai.edu.cn; Fax: (+86) 022-23503878; Tel: (+86) 022-23503878

†Electronic supplementary information (ESI) available. CCDC 1954434. For ESI and crystallographic data in CIF or other electronic format see DOI: 10.1039/d0gc03111a

‡These authors contributed equally.

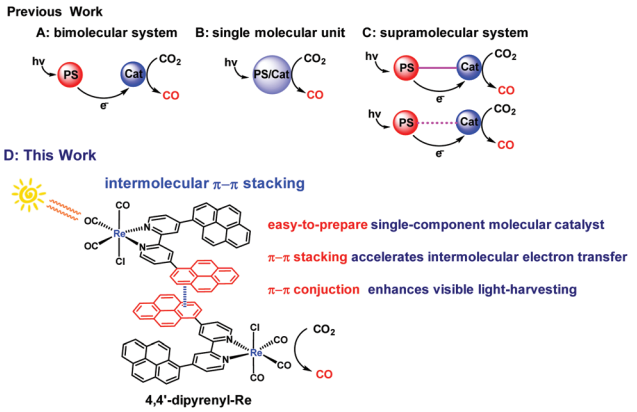

Scheme 1 Strategies for the design of catalysts for photochemical CO_2RR.

sently, developing a single-molecule photocatalyst is still a challenge.[36] As shown in previous studies,[37–40] one of the most significant points is how to maintain or even enhance the visible light-absorption ability of the targeted catalysts.

Known as an effective noncovalent intermolecular force, strong van der Waals π–π interaction is widely found in life-related biomacromolecules such as proteins, DNA and RNA,[41] and commonly promotes molecular recognition or self-assembly processes.[42,43] Moreover, the π–π stacking also facilitates the intermolecular carrier mobility in organic π-conjugated material systems.[44,45] Indeed, it has been found that noncovalent immobilization of pyrene-modified electrocatalysts on graphite surfaces or carbon nanotube electrodes for the conversion of CO_2 to fuel renders notable efficiency and selectivity.[46–48] At this point, we envision that the bifunctional pyrene group, as a photosensitizing moiety and extended π-conjugated unit, can not only enhance the visible light-harvesting capability, but also facilitate the intermolecular ET through π–π interactions, exceptionally promoting the visible light-induced CO_2 photoreduction efficiency. In this work, the widely used rhenium bipyridine complexes,[37–40,49] *e.g.* Re(bpy)$(CO)_3$Cl, are used as the model catalyst to investigate the effect of the appended pyrene groups in the ligand on the CO_2RR. The novel and easy-to-prepare catalyst, *i.e.* Re[4,4′-di(pyren-1-yl)-2,2′-bipyridine]$(CO)_3$Cl (4,4′-dipyrenyl-Re), is found to demonstrate outstanding performance for the natural light-driven CO_2RR under different weather conditions (Scheme 1D). Notably, a dramatically enhanced efficiency of this pyrene functionalized catalyst in CO_2RR can be found even at a low concentration (0.0125 mM). As expected, further improvement in the turnover number for CO (TON_{CO}) is observed after adding Ru PS, which underlines the versatile application of this methodology in photocatalytic CO_2RR.

Results and discussion

Catalyst synthesis and characterization

4,4′-Dipyrenyl-Re was synthesized *via* the reaction of 4,4′-di(pyren-1-yl)-2,2′-bipyridine and $Re(CO)_5Cl$. The structure of 4,4′-dipyrenyl-Re was verified by NMR spectroscopy and FT-IR spectroscopy, X-ray crystallography, and mass spectrometry measurement. Its crystal was recrystallized from dichloromethane and ether, and the molecular structure was refined, as shown in Fig. 1. Obviously, the intermolecular off-set π–π stacking is observed with a distance of about 3.48 Å in the packing structure of 4,4′-dipyrenyl-Re.

Visible light-driven CO_2 reduction

To validate our proposal on designing new molecular photocatalysts originating from the effect of π–π interaction, we initially performed the photocatalytic experiments in a mixture of CO_2-saturated *N*,*N*-dimethylformamide (DMF) solution with triethanolamine (TEOA) and 1,3-dimethyl-2-phenyl-2,3-dihydro-1*H*-benzo[*d*]imidazole (BIH) driven by a white-light LED. Both 4,4′-dipyrenyl-Re and Re(bpy)$(CO)_3$Cl exhibit excellent selectivity (>99%) towards CO, and only traces of H_2 (<1%) were detected, probably because triethanolamine (TEOA) can be used as a proton source, inevitably accompanied by the generation of H_2 as a byproduct (Table S6†).

No formation of HCOOH in the liquid phase can be detected by ^{1}H NMR experiments. The control experiments under an Ar atmosphere exhibit no CO production, demonstrating that CO originates from CO_2 (Table S4†). As shown in Fig. 2, a relatively high TON_{CO} (138 ± 5) is obtained when the 4,4′-dipyrenyl-Re complex is irradiated for 3 h, which then levels off to a terminal plateau. Compared to Re(bpy)$(CO)_3$Cl (TON_{CO} = 20 ± 1), the TON_{CO} for 4,4′-dipyrenyl-Re (149 ± 2) shows a more than 7-fold increase after 12 h irradiation, thus proving our hypothesis of π–π interaction effect on the large enhancement of photocatalytic efficiency. Moreover, simply mixing pyrene with the Re(bpy)$(CO)_3$Cl system has no effect on the catalytic efficiency, further demonstrating the significance of the π-expansive ligand (Table S5†). When more BIH (20 mM) is added, the amount of CO increases slightly (about 7.8 mM CO, TON_{CO} = 157 ± 5) (Table S5†). This result shows that the photocatalytic performance of CO_2 reduction is mainly limited by the decomposition and/or transformation of the Re–pyrene complex into inactive species upon two electron reduction.

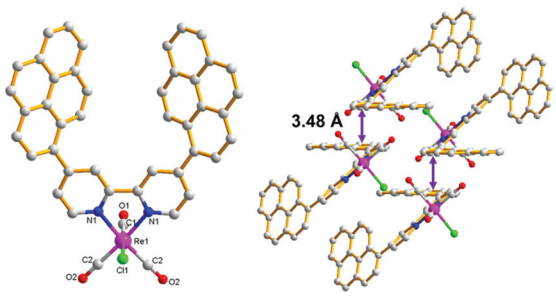

Fig. 1 X-ray crystal structure of 4,4′-dipyrenyl-Re with top (left) view and packing (right) view. Hydrogen atoms are omitted for clarity. Main bond lengths (Å) and angles (°): Re1–Cl1 2.480(3), Re1–C2 1.918(7), Re1–N1 2.176(5), N1–Re1–Cl1 84.03(15), C1–Re1–Cl1 175.7(3), and C1–Re1–N1 92.6(3). CCDC reference number: 1954434.†

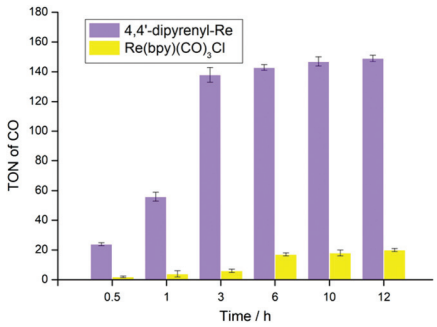

Fig. 2 TON for CO production *versus* time for 0.05 mM 4,4′-dipyrenyl-Re and 0.05 mM Re(bpy)$(CO)_3Cl$. Conditions: DMF (3 mL), TEOA (0.3 mL), 10 mM BIH; irradiated with a white LED lamp (0.60 mW cm^{-2}).

Light harvesting and redox properties

This superiority of pyrene-functionalized catalyst drove us to explore plausible reasons. At first, the visible-light absorption ability was taken into consideration. The UV-vis absorption spectra of 4,4′-dipyrenyl-Re and Re(bpy)$(CO)_3Cl$ in DMF solution are compared in Fig. 3A. It's worth noting that the molar absorptivity of 4,4′-dipyrenyl-Re (ε_{max} = 23 323 M^{-1} cm^{-1}) at about 400 nm is about six times larger than that of Re(bpy)$(CO)_3Cl$ (ε_{max} = 3754 M^{-1} cm^{-1}), which is mainly ascribed to the electron-rich expansion of the π-conjugated system through pyrene chromophores. The 4,4′-dipyrenyl-Re complex exhibits an absorption maximum at 395 nm and shows obvious bathochromic shifts in comparison with Re(bpy)$(CO)_3Cl$, indicating that the extended conjugation increases the transition probability of the metal-to-ligand charge-transfer (MLCT).[39]

From the wavelength of the onsets of UV-vis absorption spectra, the optical energy gaps of 4,4′-dipyrenyl-Re and Re(bpy)$(CO)_3Cl$ are determined as 2.71 and 3.35 eV, respectively (Table S14†). The lowest unoccupied molecular orbital (LUMO) values calculated from the onsets of the reduction potential are −3.23 and −3.12 eV for 4,4′-dipyrenyl-Re and Re(bpy)$(CO)_3Cl$, as determined by cyclic voltammetry (CV) analysis (Fig. S9†). Therefore, the highest occupied molecular orbital (HOMO) levels of both catalysts are estimated based on their LUMO levels and optical gaps, being in line with the DFT calculations (Table S14† and Fig. 3B).[50]

The next question is, what leads to the excellent optical properties of 4,4′-dipyrenyl-Re. Thus, DFT calculations were performed to compare energy levels and electron distribution from Frontier molecular orbitals of 4,4′-dipyrenyl-Re and Re(bpy)$(CO)_3Cl$ (Fig. 3B). For both Re complexes, the LUMOs are mainly localized on the bipyridine unit. However, the HOMOs are distributed on the Re center, such as Re(bpy)$(CO)_3Cl$, as well as on the appending pyrene groups. A narrower energy gap between the LUMO and HOMO (Fig. 3C) is found for 4,4′-dipyrenyl-Re. Consequently, pyrene units with a large extended conjugation and electron-donating character can lower the LUMO level and effectively elevate the HOMO level for this catalyst, leading to the narrower energy gap, enhancing the light-harvesting capability. Moreover, the driving force for the sacrificial reductants was also discussed to study the thermodynamic process of CO_2RR. For the 4,4′-dipyrenyl-Re complex, we found that the yield of CO was distinctly reduced in the absence of BIH through the control experiments (Table S7†), although TEOA itself was considered as a base in addition to being an electron donor.[33] The main reason is that the redox potential of TEOA is almost close to the HOMO value of 4,4′-dipyrenyl-Re (Fig. 3C), which indicates that the ET from TEOA to pyrene moieties of this catalyst is limited.[51] Thus, the use of BIH as the sacrificial reductant and TEOA, a "magic" reagent,[52] is a feasible strategy to effectively avoid the thermodynamic limitation of photocatalytic CO_2RR. According to previous reports, TEOA, acting as a base to capture a proton from $BIH^{\bullet+}$, a proton source, or a CO_2 absorbent to form the TEOA-CO_2 adduct, was considered as a main component of the Re complexes during the photocatalytic formation of CO.[53,54]

Investigation of the intermolecular π–π interactions

As is well known, intermolecular π–π stacking has the ability to accelerate intermolecular ET.[55,56] Despite π–π stacking being identified in the crystal of 4,4′-dipyrenyl-Re, the intermolecular force pattern of this catalyst in solution should be further

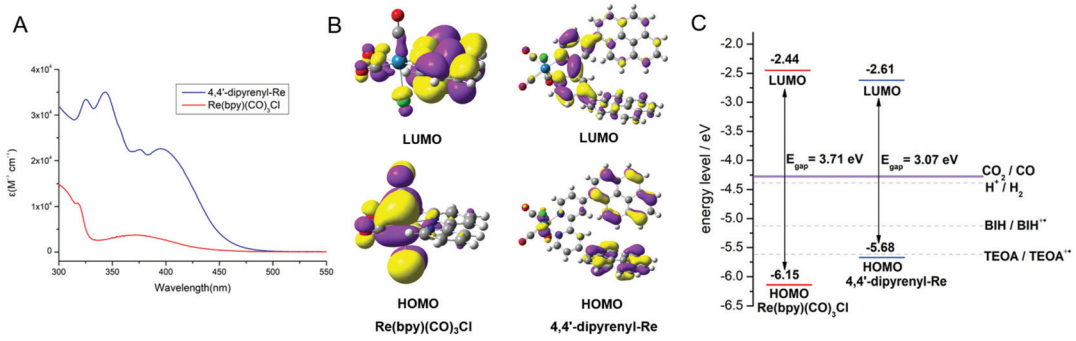

Fig. 3 Optical and electrochemical properties of the Re(bpy)$(CO)_3Cl$ and 4,4′-dipyrenyl-Re. (A) UV-vis absorption of the Re(bpy)$(CO)_3Cl$ and 4,4′-dipyrenyl-Re in DMF at rt; (B) shape of HOMOs and LUMOs of Re(bpy)$(CO)_3Cl$ and 4,4′-dipyrenyl-Re; and (C) HOMO and LUMO energy levels of Re(bpy)$(CO)_3Cl$ and 4,4′-dipyrenyl-Re, together with redox potentials (eV) of CO_2/CO and electron donors BIH and TEOA.

investigated. Thus, the photoluminescence (PL) spectra of 4,4′-dipyrenyl-Re were measured at different concentrations in DMF solution. The fluorescence intensity of 4,4′-dipyrenyl-Re dramatically decreases when the concentration is increased from 0.0125 mM to 0.2 mM (Fig. 4A). At the same time, the appearance of an additional emission peak at 650 nm from the Re–pyrene excimer was confirmed by time-resolved emission, and the emission lifetime was found to be 0.141 ns (Fig. S4†). In sharp contrast, only a small decrease can be observed in the same concentration range for $Re(bpy)(CO)_3Cl$ (Fig. S3†). Clearly, the severe aggregation-caused quenching (ACQ) mainly originates from the π–π stacking of 4,4′-dipyrenyl-Re in DMF solution.

Furthermore, the intermolecular π–π interaction of 4,4′-dipyrenyl-Re in solution was verified by variable-temperature NMR spectroscopy. The ^1H NMR spectra of 4,4′-dipyrenyl-Re in DMSO-*d*6 manifest obvious upfield shifts with increasing temperature for the pyrene protons. For instance, the typical peak for pyrene groups shifts from δ = 9.35 to 9.29 ppm when the temperature increases from 25 °C to 65 °C (Fig. 4B), indicating that the π–π stacking is impeded between pyrene moieties by heating. However, only inconspicuous shift can be found for the protons of bipyridine. The above observations suggest that the pyrene group leads to the π–π stacking of 4,4′-dipyrenyl-Re other than bipyridine.

It is well known that decreasing the catalyst concentration is an effective and feasible way to evaluate the activity, because intermolecular ET and non-covalent interactions (such as intermolecular π–π interactions) will be limited by the low catalyst concentration. We then investigated the concentration effects on the photocatalytic performance (Table S8†). Compared with $Re(bpy)(CO)_3Cl$, 4,4′-dipyrenyl-Re showed a significant increase in CO yield at all concentrations examined in this work (Fig. 5). The main reason would be that the fraction of absorbed photons of Re–pyrene catalyst was significantly higher than that of $Re(bpy)(CO)_3Cl$ at different concentrations as shown in the Fig. S2A.† For example, when the concentration is 0.0125 mM, the CO yield of 4,4′-dipyrenyl-Re is 26 times higher than that of $Re(bpy)(CO)_3Cl$.

More importantly, unlike $Re(bpy)(CO)_3Cl$, 4,4′-dipyrenyl-Re exhibits less sensitivity to the concentration. When the concentration is reduced from 0.1 to 0.0125 mM, the yield of CO decreases only by 72.6% for 4,4′-dipyrenyl-Re that is even lower than the reduced concentration ratio (87.5%) (Table S9†).

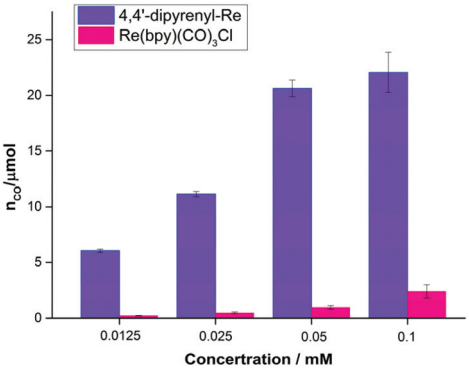

Fig. 5 TON for CO production *versus* catalyst concentration for 4,4′-dipyrenyl-Re and $Re(bpy)(CO)_3Cl$. Conditions: DMF (3 mL), TEOA (0.3 mL), 10 mM BIH; irradiated with a white LED (0.60 mW cm^{-2}).

The effect of fraction of absorbed photons on the molar amount of CO was further explored (Fig. S2B†), we found that Re–pyrene could produce approximately three times more CO than $Re(bpy)(CO)_3Cl$ at the same fraction of absorbed photons (such as 0.5), which indicated that the high activity of Re–pyrene may be due to the improvement of intermolecular ET. Thus, increasing the light harvesting ability and intermolecular π–π interaction of the Re catalyst leads to high performance at low concentrations, which is remarkably superior to previously reported molecular systems (Table S13†). In contrast, in the case of $Re(bpy)(CO)_3Cl$, the CO yield is reduced by more than 90% when the concentration is decreased from 0.1 to 0.0125 mM (Table S9†), presumably owing to the impediment of ET and weak absorbance under low catalyst concentrations. A Re complex and another Re molecule interact less frequently and the potential degradation of either species is more competitive at low concentrations.[38] In addition, it should be mentioned that the quantum yields of CO formation (Φ_{CO}) are 46.6 ± 3% for 4,4′-dipyrenyl-Re (n_{CO} = 29.08 ± 2 μmol) and 7.3 ± 2% for $Re(bpy)(CO)_3Cl$ (n_{CO} = 4.56 ± 1.4 μmol) after irradiation for 0.5 h by a xenon lamp (λ = 420 nm, 0.82 mW cm^{-2}) (Table S10†). These results suggest that 4,4′-dipyrenyl-Re has a significant enhancement in the photocatalytic activity compared to $Re(bpy)(CO)_3Cl$.

Transient absorption spectra were investigated to further explore the mechanism. As shown in Fig. S8A,† 4,4′-dipyrenyl-Re in degassing DMF exhibited a strong bleaching peak at 300–400 nm upon pulsed laser excitation at 410 nm, corresponding to its ground state absorption. 4,4′-Dipyrenyl-Re showed two positive absorption bands at around 500 and 558 nm, and its lifetime was determined as 117.7 μs (Fig. S8D†), which may be attributed to the monomer excited state and the aggregated excited Re–pyrene species. By the addition of BIH, a species of reduced 4,4′-dipyrenyl-Re was formed with a decay of 35.1 μs under an Ar atmosphere (Fig. S8B and S8E†), supporting an electron transfer pathway

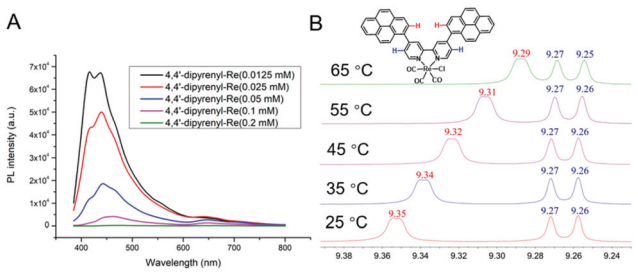

Fig. 4 Photoluminescence (PL) and variable-temperature ^1H NMR characteristics of 4,4′-dipyrenyl-Re. (A) Photoluminescence experiments at different concentrations of 4,4′-dipyrenyl-Re and (B) partial variable temperature ^1H NMR of 4,4′-dipyrenyl-Re in DMSO-*d*6.

from BIH to the excited Re–pyrene species. In addition, it is worth noting that reduced 4,4′-dipyrenyl-Re returned quickly to the baseline with a decay of 21.0 μs under a CO_2 atmosphere (Fig. S8C and S8F†). Based on above experimental results and previous reports,[57,58] the proposed pathway is depicted in Fig. 6. We speculate that the CO_2RR most probably initiates *via* reductive quenching of the excited state of the Re(I) unit with the electron donor (BIH). The π–π stacking interaction, one of the common noncovalent forces, efficiently facilitates intermolecular ET of pyrene moieties of the 4,4′-dipyrenyl-Re complex. Thus, the one-electron-reduced Re-pyrene$^{\bullet-}$ could be consumed more quickly *via* intermolecular ET, inhibiting back-electron transfer from the reduced state of Re species to the oxidized state of the sacrificial electron donor, and ultimately improving the photocatalytic efficiency of CO_2RR. Intermolecular ET may proceed from the photochemically formed Re-pyrene$^{\bullet-}$ to another proximal Re–pyrene catalytic center by intermolecular π–π interaction of pyrene units, and CO_2RR takes place at the Re center to catalyze CO_2-to-CO conversion. In short, π–π interaction and extension of the π-conjugated system dramatically improve ET and visible light-harvesting, thereby leading to efficient photocatalytic performance in solar energy-driven CO_2 reduction.

Application under natural conditions

Sunlight-driven CO_2 reduction could be promising, but still remains an elusive goal for photocatalytic CO_2 reduction. Having identified the superiority of 4,4′-dipyrenyl-Re in visible-light absorption and intermolecular ET, we subjected 4,4′-dipyrenyl-Re and Re(bpy)$(CO)_3$Cl to CO_2 reduction under sunlight under different weather conditions (Table S11†). These experiments were conducted near a window inside the laboratory from 11:00 am to 2:00 pm (Fig. 7). We found that sunny sunlight (about 0.75 mW cm^{-2}) and the long-arc xenon lamp (λ > 400 nm, 8.34 mW cm^{-2}) and xenon lamp (λ = 420 nm, 0.82 mW cm^{-2}) give rise to almost the same results for both catalysts, while cloudy sunlight (about 0.32 mW cm^{-2}) performs similar to a white LED. Notably, TON_{CO} for 4,4′-dipyrenyl-Re on a sunny day reaches up to 350 ± 36, but Re(bpy)$(CO)_3$Cl exhibits much lower activity (TON_{CO} = 22 ± 2) under identical conditions. Although performance is reduced on a cloudy day, TON_{CO} for 4,4′-dipyrenyl-Re is 40-fold higher than that for Re(bpy)$(CO)_3$Cl. Then, the reactions for longer time (6 hours) at a Re–pyrene concentration of 0.0125 mM under a white LED light as well as a long-arc xenon lamp were also performed. We found that the amount of CO increased slightly when the reaction time was prolonged driven by white LED light (0.60 mW cm^{-2}) or long-arc xenon lamp (8.34 mW cm^{-2}) (Table S11†). These results suggest that the change of light intensity more/less leads to the decomposition of the Re–pyrene catalyst. Therefore, the main factors affecting photocatalytic efficiency of Re–pyrene catalyst would be light intensity and light absorption performance.

To further broaden the application of this method in photocatalytic CO_2RR, multicomponent systems using Ru(bpy)$_3$(Cl)$_2$·6H$_2$O (RuBPY) as PS were also investigated. First, without RuBPY, Re(bpy)$(CO)_3$Cl has been deactivated when the concentration is as low as 3.125 μM, while 4,4′-dipyrenyl-Re can still give a TON_{CO} of 76 ± 3 (Fig. 8 and Table S12†). The activities are greatly boosted by additional PS (RuBPY), and 4,4′-dipyrenyl-Re (TON_{CO} = 1367 ± 32) shows higher efficiency than Re(bpy)$(CO)_3$Cl (TON_{CO} = 840 ± 28). Then, the rates of the kinetic process for both systems were determined through Stern–Volmer analysis (Fig. S5 and S6†). It is found that the

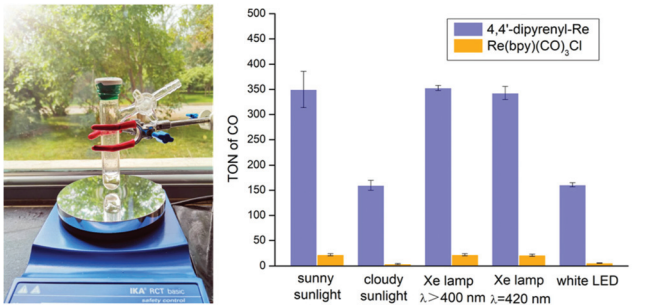

Fig. 7 Photocatalytic CO_2 reduction driven by natural light. CO_2 photo-reduction by 4,4′-dipyrenyl-Re (0.0125 mM) and Re(bpy)$(CO)_3$Cl (0.0125 mM) in 3 h driven by different light sources.

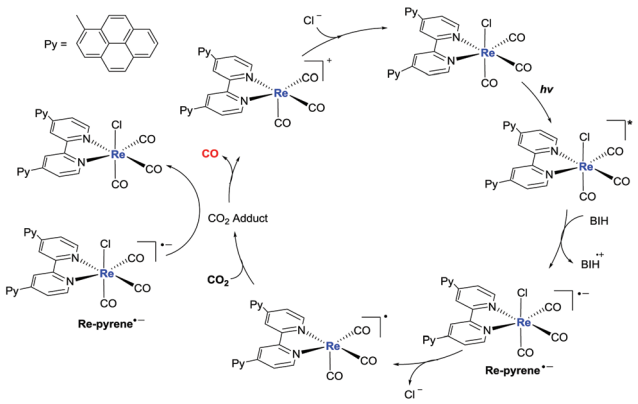

Fig. 6 Proposed pathway for such a photochemical CO_2 conversion.

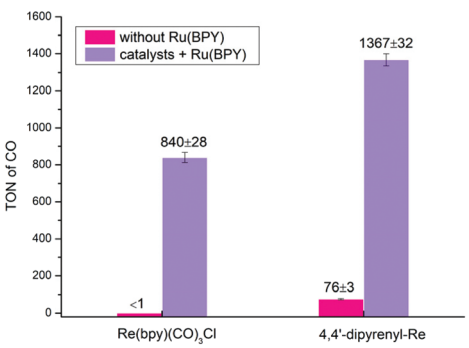

Fig. 8 CO_2 photo-reduction by 4,4′-dipyrenyl-Re or Re(bpy)$(CO)_3$Cl (3.125 μM) as catalyst and RuBPY (0.5 mM) as PS in 3 h driven by a long-arc xenon lamp (8.34 mW cm^{-2}).

fluorescence emission of RuBPY was oxidatively quenched by both catalysts with quenching constants (k_q) of 3.45×10^{10} M^{-1} s^{-1} for 4,4′-dipyrenyl-Re, which is much larger than that for Re(bpy)$(CO)_3$Cl (1.07×10^9 M^{-1} s^{-1}). Moreover, Stern–Volmer analysis also revealed that BIH quenches RuBPY fluorescence with corresponding quenching rate constants of 5.1×10^9 M^{-1} s^{-1} (Fig. S7†). This pathway could be dominant because the concentration of BIH is much greater than that of the Re–pyrene catalyst. These results imply that the mechanism with reductive quenching in this multi-component system would be favourable.

The ET process also plays a significant role in the electroreduction of CO_2. We wonder if our method can be used to improve the efficiency of electrochemical CO_2 reduction. First, the redox behaviors of 4,4′-dipyrenyl-Re and Re(bpy)$(CO)_3$Cl were analyzed by CV in DMF solutions under an Ar atmosphere, displaying initial $1e^-$ reduction potentials at −1.69, −1.79 V, respectively (Fig. S9 and Table S15†). By introducing pendant pyrene groups, the reduction potential of 4,4′-dipyrenyl-Re with a 0.1 V positive shift compared to that of Re(bpy)$(CO)_3$Cl, and thus the 4,4′-dipyrenyl-Re complex is more easily reduced. Moreover, the catalytic current response of both Re complexes for electrocatalytic CO_2 reduction was investigated under saturated CO_2 conditions (Fig. 9). Most notably, the pyrene functionalized catalyst exhibits reductive current enhancement with a higher i_{cat} (catalytic peak current)/i_p (initial $1e^-$ reduction under Ar conditions) value of 13.6 as compared to Re(bpy)$(CO)_3$Cl (3.3) (Table 1), strongly indicating the remarkable role of the pendant pyrene groups to facilitate ET during CO_2 reduction.

The quantity i_{cat}/i_p can act as a useful tool for determining catalytic performance by CVs, but this is a rough measure. Ideally, the catalytic CV assumes an "S-shaped" wave independent of the scanning rate, where the platform current can be used to determine the intrinsic catalytic rate constant (k_{cat}). However, a peak-shaped response occurs commonly due to interference of "secondary phenomena" such as the catalyst deactivation or substrate consumption.[60] One method to counter these phenomena is to increase the scan rate and thereby reduce the passing charge, so as to get back to an S-shaped current potential response and derive the rate constant k_{cat} (s^{-1}) from the S-shaped current plateau, as shown in eqn (1),[61,62] where n' is the catalyst equivalents required per turnover, n is the number of electrons transferred in the catalytic process, ν is the scan rate, R is the ideal gas constant, and T is the temperature. The k_{cat} (s^{-1}) values are equal to the maximum turnover frequency (TOF_{max}) under these conditions. For 4,4′-dipyrenyl-Re and Re(bpy)$(CO)_3$Cl complexes through increasing the scan rate to obtain the plateau (S-shaped) current, the k_{cat} (s^{-1}) values are calculated as 967 and 150 s^{-1}, respectively (Fig. 10 and Table 1). Therefore, with faster ET efficiency, the pyrenyl functionalized catalyst results in a higher TOF_{max} relative to unmodified Re(bpy)$(CO)_3$Cl.

$$\frac{i_{cat}}{i_p} = \frac{1}{0.446}\sqrt{\frac{RT}{nF\nu}n'k_{cat}} \quad (1)$$

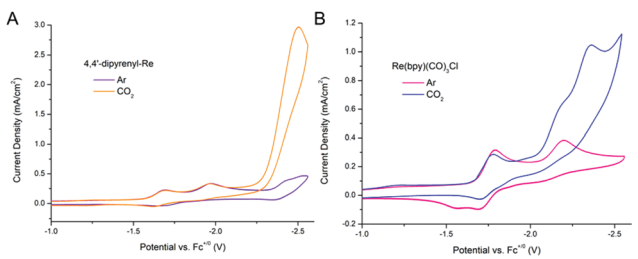

Fig. 9 Electrocatalytic performances of rhenium complexes. Cyclic voltammetry of 1 mM 4,4′-dipyrenyl-Re (A) and Re(bpy)$(CO)_3$Cl (B) in argon- and CO_2-saturated DMF/0.1 M NBu_4PF_6 solutions recorded at 0.1 V s^{-1}.

Table 1 Catalytic descriptors for rhenium complexes under CO_2 conditions

Catalyst	$E_{cat/2}$ [a]	η [b]	i_{cat}/i_p [c]	k_{cat} [d] (s^{-1})
4,4′-Dipyrenyl-Re	−2.40	1.67	13.6	967 (25)
Re(bpy)$(CO)_3$Cl	−2.23	1.50	3.3	150 (5)

[a] The value at half of the catalytic current. [b] Overpotentials were determined by the expression $\eta = |E_{cat/2} - E^{\circ}_{CO_2/CO}(DMF)|$, $E^{\circ}_{CO_2/CO}(DMF) = -0.73$ V *vs.* $Fc^{+/}0$.[59] [c] Ratio between the peak current under CO_2 (i_{cat}) and the initial $1e^-$ reduction under argon conditions (i_{cat}/i_p) at a scan rate of 0.1 V s^{-1}. [d] Scan rate is given in parentheses (V s^{-1}).

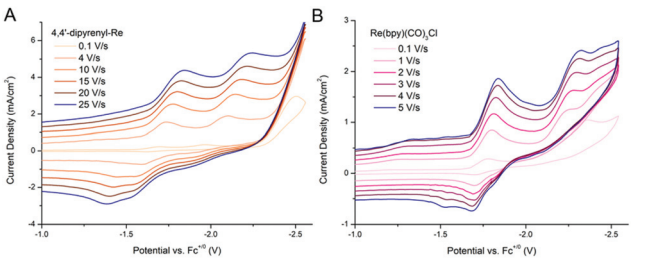

Fig. 10 Determination of the catalytic rate constant. Catalytic scan rate dependence studies for the 4,4′-dipyrenyl-Re (A) and Re(bpy)$(CO)_3$Cl (B) complexes in CO_2-saturated DMF/0.1 M NBu_4PF_6 solutions.

Conclusions

In conclusion, we have designed an easy-to-prepare single-molecule catalyst system comprising a Re complex with covalently linked pyrene groups without additional photosensitizers for natural light-driven photocatalytic CO_2 reduction under different weather conditions. A series of experimental, spectroscopic and theoretical studies demonstrate that π–π interactions and extension of the π-conjugated system originating from pyrene groups dramatically improve the electron transfer efficiency and the visible light-harvesting ability. To our delighted, 4,4′-dipyrenyl-Re exhibits high efficiency in the sunny sunlight-driven CO_2-to-CO conversion with a high turnover number (TON_{CO} = 350 ± 36) and Φ_{CO} is up to 46.6 ± 3%.

To the best of our knowledge, this is the first example to realize CO_2RR directly under the sun by using a single-molecule catalyst. More importantly, this methodology can also be applied to multicomponent systems with a remarkable increase in the TON_{CO} of up to 1367 ± 32. In addition, due to the accelerated ET efficiency, pyrenyl functionalized Re catalyst with higher electrocatalytic activity (TOF_{max} = 967 s^{-1}) toward CO_2 reduction compared to Re(bpy)$(CO)_3$Cl. We believe that this strategy will pave the way for designing catalysts in photo- and electro-chemical CO_2RR. Our laboratory will pay more attention to novel intermolecular ET related materials using CO_2 from flue gas or atmospheric CO_2 [63,64] for photocatalytic CO_2 reduction.

Experimental section

Materials

N,*N*-Dimethylformamide (DMF, J&K, 99.8%), 4,4′-dibromo-2,2′-bipyridine (Meryer, 97%), 1-pyrenylboronic acid (Bide, 97%), $Pd(PPh_3)_4$ (J&K, 98%), and rhenium pentacarbonyl chloride (Acros Organics, 98%) were commercially available and used without further purification. The solvents (toluene and tetrahydrofuran) used for reactions were distilled under argon after drying over an appropriate drying agent. Argon (purity ≥99.998%) and $^{12}CO_2$ (purity ≥99.999%) were from Tianjin HAOLUN.

Synthesis of Re(bpy)$(CO)_3$Cl and 1,3-dimethyl-2-phenyl-2,3-dihydro-1*H*-benzo[*d*]-imidazole (BIH) were prepared according to the literature.[65,66]

Synthesis of 4,4′-di(pyren-1-yl)-2,2′-bipyridine

A mixture of 4,4′-dibromo-2,2′-bipyridine (157 mg, 0.5 mmol), 1-pyrenylboronic acid (270 mg, 1.1 mmol), Na_2CO_3 (159 mg, 1.5 mmol) and $Pd(PPh_3)_4$ (29 mg, 0.025 mmol) in THF/H_2O (6 mL/3 mL) was stirred at 75 °C for 12 h under an Ar atmosphere. The reaction mixture was allowed to cool to room temperature, and water (5 mL) and dichloromethane (10 mL) were added. The organic phase was collected, and the solid was suspended in dichloromethane and filtered to give crude 4,4′-di(pyren-1-yl)-2,2′-bipyridine as a pale yellow powder, which was used without further purification. Due to the extremely low solubility of 4,4′-dipyrenyl-2,2′-bipyridine in common NMR solvents, such as $CDCl_3$, CD_3CN, DMSO-d_6, or C_6D_6, a detailed spectroscopic NMR investigation was not possible. The precursor 4,4′-di(pyren-1-yl)-2,2′-bipyridine was confirmed by high-resolution mass spectrometry and FT-IR spectroscopy. 4,4′-Di(pyren-1-yl)-2,2′-bipyridine: pale yellow solid (232 mg, 83% yield). HRMS (ESI) Calcd for $C_{24}H_{42}N_2$: 556.1939; Found: 556.2768. IR (KBr) ν(C–H): 3038 cm^{-1}, ν(C═N): 1590 cm^{-1}.

Synthesis of Re[4,4′-di(pyren-1-yl)-2,2′-bipyridine](CO)$_3$Cl (4,4′-dipyrenyl-Re)

A mixture of $Re(CO)_5Cl$ (18 mg, 0.05 mmol) and 4,4′-di(pyren-1-yl)-2,2′-bipyridine (28 mg, 0.05 mmol) was dissolved in 40 mL toluene solution under an Ar atmosphere. The mixture was refluxed at 110 °C overnight. The resulting mixture was extracted with dichloromethane (3 × 15 mL), dried over anhydrous Mg_2SO_4, filtered and the solvent was removed *in vacuo*, and the residue was subjected to column chromatography to afford the pure product (hexane : dichloromethane = 1 : 2, TLC: R_f = 0.25). Re[4,4′-di(pyren-1-yl)-2,2′-bipyridine](CO)$_3$Cl: orange yellow solid (32 mg, 74% yield). ^{1}H NMR (400 MHz, DMSO) δ 9.35 (s, 2H), 9.26 (d, J = 5.7 Hz, 2H), 8.45 (d, J = 8.0 Hz, 2H), 8.37 (d, J = 14.7 Hz, 2H), 8.37 (s, 2H), 8.30–8.25 (m, 10H), 8.24–8.10 (m, 4H) ppm. HRMS (ESI) Calcd for $C_{45}H_{24}N_2O_3Re$ $(M - Cl)^+$ 827.1344; Found: 827.1344. IR (KBr) ν(CO): 2017 cm^{-1}, 1910 cm^{-1}, 1888 cm^{-1}. Anal. Calcd for $C_{45}H_{24}ClN_2O_3Re$: C, 62.68; H, 2.81; N, 3.25. Found: C, 62.36; H, 3.15; N, 2.87.

Photocatalytic experiments

Photocatalytic CO_2 reduction was performed on a 10 mL Schlenk tube containing the Re catalyst, TEOA (0.3 mL), BIH (10 mM), and 3 mL DMF mixed solution under a CO_2 atmosphere at room temperature. After the reaction system was purged with CO_2 (1 atm) for three freeze–pump–thaw cycles, the reaction mixture was stirred with a magnetic bar and irradiated under a white LED light (9 W) or a long-arc xenon lamp or near a window inside a room under different weather conditions. After the reaction, partial gaseous products (1 mL) were taken from the tube using a syringe, and then detected by gas chromatography (GC, FuLi 9790II) with a TCD detector. The volume of carbon dioxide can be calculated by injecting water into the 10 mL Schlenk tube, and then we used the ideal gas law ($PV = nRT$) to figure out the moles of CO_2 in the Schlenk tube. All the photocatalytic reactions were repeated three times to confirm the reliability of the data. The turnover numbers (TONs) are based on the Re catalysts. Only traces of H_2 were detected. In the liquid phase, no formation of HCOOH can be observed by ^{1}H NMR experiments. Products below the detectable limit are labelled as NA (see the ESI†).

Determination of the quantum yield

The photon flux was determined by standard ferrioxalate actinometry.[67] To determine the photon flux of the xenon lamp (0.82 mW cm^{-2}), the ferrioxalate solution was placed in a cuvette and irradiated at λ = 420 nm. After irradiation, the phenanthroline solution was added to the cuvette and the mixture was allowed to stir in the dark for 1 h to promote the ferrous ions to completely coordinate with phenanthroline. The absorbance of the solution was measured at 510 nm. A nonirradiated sample was also prepared and the absorbance at 510 nm was measured. It is noteworthy that CO formation from CO_2 requires two electrons, one-electron-reduced Re-pyrene$^{\bullet-}$ should be produced by the second excitation. The radical species BI$^\bullet$ that is produced *via* deprotonation from the one-electron-oxidized BIH$^{\bullet+}$ is also a second-electron donor candidate. Therefore, the reaction path should be a photon absorption, followed by an electron transfer. The quantum

yield (Φ) was determined using eqn (2), where the photon flux is 6.93×10^{-8} einstein per s.

$$\Phi(\%) = \frac{\text{number of CO molecules formed} \times 2}{\text{number of incident photons}} \times 100\% \quad (2)$$

Single-crystal X-ray analysis and photoelectrochemical measurements

X-ray crystallographic analyses were performed on a Rigaku Saturn 724 CCD diffractometer using graphite-monochromated Mo Kα radiation. UV-visible spectra were recorded at room temperature on a Shimadzu UV-2450 spectrophotometer. Fluorescence spectra were obtained with a Varian Cary Eclipse spectrometer. Emission intensities used for Stern–Volmer analysis were taken at 630 nm, *i.e.*, the emission maximum of $Ru(bpy)_3(Cl)_2{\cdot}6H_2O$. Infrared (IR) spectra were recorded on a Bruker Tensor 27 FT-IR spectrophotometer with KBr pellets. Cyclic voltammograms were recorded on BAS Epsilon with a three electrode setup: 3 mm diameter glassy carbon working electrode, non-aqueous reference electrode ($Ag/AgNO_3$ in CH_3CN solution), and platinum foil counter electrode. CVs of 1.0 mM catalyst recorded at 0.1 V s^{-1} in DMF (0.1 M NBu_4PF_6). Transient absorption spectra were measured on the LP980 laser flash photolysis instrument (Edinburgh, UK). FL lifetime was determined using a time-resolved confocal FL instrument (MicroTime 200, PicoQuant, Berlin, Germany). All potentials were referenced internally at the end of the experiments to the ferrocenium/ferrocene ($Fc^{+/0}$) couple.

Conflicts of interest

The authors declare no competing interests.

Acknowledgements

This work was financially supported by the National Natural Science Foundation of China (21672119 and 21975135), the National Key R&D Program of China (2016YFA0602900), and the China Postdoctoral Science Foundation (2018M641624). We do greatly appreciate the support from Prof. Tong Bu Lu, Dr Song Guo, and Ping Wang (Tianjin University of Technology) in photoluminescence lifetime and transient absorption measurement.

References

1 M. Meinshausen, N. Meinshausen, W. Hare, S. C. B. Raper, K. Frieler, R. Knutti, D. J. Frame and M. R. Allen, *Nature*, 2009, **458**, 1158–1162.
2 T. R. Karl and K. E. Trenberth, *Science*, 2003, **302**, 1719–1723.
3 C. Zhou, J. Shi, W. Zhou, K. Cheng, Q. Zhang, J. Kang and Y. Wang, *ACS Catal.*, 2020, **10**, 302–310.
4 Q. Guo, S.-G. Xia, X.-B. Li, Y. Wang, F. Liang, Z.-S. Lin, C.-H. Tung and L.-Z. Wu, *Chem. Commun.*, 2020, **56**, 7849–7852.
5 W. Zhou, K. Cheng, J. Kang, C. Zhou, V. Subramanian, Q. Zhang and Y. Wang, *Chem. Soc. Rev.*, 2019, **48**, 3193–3228.
6 L. Lu, X.-F. Sun, J. Ma, D.-X. Yang, H.-H. Wu, B.-X. Zhang, J.-L. Zhang and B.-X. Han, *Angew. Chem., Int. Ed.*, 2018, **57**, 14149–14153.
7 X. He, Y. Cao, X.-D. Lang, N. Wang and L.-N. He, *ChemSusChem*, 2018, **11**, 3382–3387.
8 J. Artz, T. E. Müller, K. Thenert, J. Kleinekorte, R. Meys, A. Sternberg, A. Bardow and W. Leitner, *Chem. Rev.*, 2018, **118**, 434–504.
9 Y. Wang and D. J. Darensbourg, *Coord. Chem. Rev.*, 2018, **372**, 85–100.
10 S. Xie, Q. Zhang, G. Liu and Y. Wang, *Chem. Commun.*, 2016, **52**, 35–59.
11 M.-Y. He, Y.-H. Sun and B.-X. Han, *Angew. Chem., Int. Ed.*, 2013, **52**, 9620–9633.
12 M. E. Dry, *Catal. Today*, 2002, **71**, 227–241.
13 D. G. Nocera, *Acc. Chem. Res.*, 2017, **50**, 616–619.
14 I. Dincer and C. Acar, *Int. J. Energy Res.*, 2015, **39**, 585–606.
15 N. S. Lewis and D. G. Nocera, *Proc. Natl. Acad. Sci. U. S. A.*, 2006, **103**, 15729–15735.
16 G. Lan, Z. Li, S. S. Veroneau, Y.-Y. Zhu, Z. Xu, C. Wang and W. Lin, *J. Am. Chem. Soc.*, 2018, **140**, 12369–12373.
17 M. Zhang, M. Lu, Z.-L. Lang, J. Liu, M. Liu, J.-N. Chang, L.-Y. Li, L.-J. Shang, M. Wang, S.-L. Li and Y.-Q. Lan, *Angew. Chem.*, 2020, **59**, 6500–6506.
18 M. Lu, J. Liu, Q. Li, M. Zhang, M. Liu, J.-L. Wang, D.-Q. Yuan and Y.-Q. Lan, *Angew. Chem., Int. Ed.*, 2019, **58**, 12392–12397.
19 A. V. Akimov, A. J. Neukirch and O. V. Prezhdo, *Chem. Rev.*, 2013, **113**, 4496–4565.
20 D. R. Weinberg, C. J. Gagliardi, J. F. Hull, C. F. Murphy, C. A. Kent, B. C. Westlake, A. Paul, D. H. Ess, D. G. McCafferty and T. J. Meyer, *Chem. Rev.*, 2012, **112**, 4016–4093.
21 S. Horiuchi, Y. Okimoto, R. Kumai and Y. Tokura, *Science*, 2003, **299**, 229–232.
22 T. Aida, E. W. Meijer and S. I. Stupp, *Science*, 2012, **335**, 813–817.
23 A. Ajayaghosh and V. K. Praveen, *Acc. Chem. Res.*, 2007, **40**, 644–656.
24 K. V. Rao and S. J. George, *Chem. – Eur. J.*, 2012, **18**, 14286–14291.
25 D. Hong, T. Kawanishi, Y. Tsukakoshi, H. Kotani, T. Ishizuka and T. Kojima, *J. Am. Chem. Soc.*, 2019, **141**, 20309–20317.
26 D.-C. Liu, H.-J. Wang, T. Ouyang, J.-W. Wang, L. Jiang, D.-C. Zhong and T.-B. Lu, *ACS Appl. Energy Mater.*, 2018, **1**, 2452–2459.
27 T. Ouyang, H.-H. Huang, J.-W. Wang, D.-C. Zhong and T.-B. Lu, *Angew. Chem., Int. Ed.*, 2017, **56**, 738–743.
28 H. Takeda, C. Cometto, O. Ishitani and M. Robert, *ACS Catal.*, 2016, **7**, 70–88.

29 H. Takeda, H. Koizumi, K. Okamoto and O. Ishitani, *Chem. Commun.*, 2014, **50**, 1491–1493.
30 J. Bonin, M. Robert and M. Routier, *J. Am. Chem. Soc.*, 2014, **136**, 16768–16771.
31 Y. Yamazaki, K. Ohkubo, D. Saito, T. Yatsu, Y. Tamaki, S. Tanaka, K. Koike, K. Onda and O. Ishitani, *Inorg. Chem.*, 2019, **58**, 11480–11492.
32 Y. Kuramochi, O. Ishitani and H. Ishida, *Coord. Chem. Rev.*, 2018, **373**, 333–356.
33 Y. Tamaki and O. Ishitani, *ACS Catal.*, 2017, **7**, 3394–3409.
34 B. Gholamkhass, H. Mametsuka, K. Koike, T. Tanabe, M. Furue and O. Ishitani, *Inorg. Chem.*, 2005, **44**, 2326–2336.
35 P. L. Cheung, S. C. Kapper, T. Zeng, M. E. Thompson and C. P. Kubiak, *J. Am. Chem. Soc.*, 2019, **141**, 14961–14965.
36 T. J. Whittemore, C. Xue, J. Huang, J. C. Gallucci and C. Turro, *Nat. Chem.*, 2020, **12**, 180–185.
37 K.-H. Chen, N. Wang, Z.-W. Yang, S.-M. Xia and L.-N. He, *ChemSusChem*, 2020, DOI: 10.1002/cssc.202000698.
38 N. P. Liyanage, W. Yang, S. Guertin, S. S. Roy, C. A. Carpenter, R. E. Adams, R. H. Schmehl, J. H. Delcamp and J. W. Jurss, *Chem. Commun.*, 2019, **55**, 993–996.
39 D. R. Whang, D. H. Apaydin, S. Y. Park and N. S. Sariciftci, *J. Catal.*, 2018, **363**, 191–196.
40 A. Maurin, C.-O. Ng, L. Chen, T.-C. Lau, M. Robert and C.-C. Ko, *Dalton Trans.*, 2016, **45**, 14524–14529.
41 C. A. Hunter, *J. Mol. Biol.*, 1993, **230**, 1025–1054.
42 M. P. Parker, C. A. Murray, L. R. Hart, B. W. Greenland, W. Hayes, C. J. Cardin and H. M. Colquhoun, *Cryst. Growth Des.*, 2018, **18**, 386–392.
43 W. Wang, J. J. Han, L.-Q. Wang, L.-S. Li, W. J. Shaw and A. D. Q. Li, *Nano Lett.*, 2003, **3**, 455–458.
44 Y. Liu, W. Hao, H. Yao, S. Li, Y. Wu, J. Zhu and L. Jiang, *Adv. Mater.*, 2018, **30**, 1705377.
45 T. M. Figueira-Duarte and K. Müllen, *Chem. Rev.*, 2011, **111**, 7260–7314.
46 J. D. Blakemore, A. Gupta, J. J. Warren, B. S. Brunschwig and H. B. Gray, *J. Am. Chem. Soc.*, 2013, **135**, 18288–18291.
47 P. Kang, S. Zhang, T. J. Meyer and M. Brookhart, *Angew. Chem., Int. Ed.*, 2014, **53**, 8709–8713.
48 S. Sinha, A. Sonea, W. Shen, S. S. Hanson and J. J. Warren, *Inorg. Chem.*, 2019, **58**, 10454–10461.
49 J. Hawecker, J.-M. Lehn and R. Ziessel, *J. Chem. Soc., Chem. Commun.*, 1983, 536–538.
50 M. J. Frisch, *et al.*, *Gaussian 09, revision D.01*, Gaussian, 2009.
51 F. M. Wisser, M. Duguet, Q. Perrinet, A. C. Ghosh, M. Alves-Favaro, Y. Mohr, C. Lorentz, E. A. Quadrelli, R. Palkovits, D. Farrusseng, C. Mellot-Draznieks, V. de Waele and J. Canivet, *Angew. Chem.*, 2020, **59**, 5116–5122.
52 T. Morimoto, T. Nakajima, S. Sawa, R. Nakanishi, D. Imori and O. Ishitani, *J. Am. Chem. Soc.*, 2013, **135**, 16825–16828.
53 T. Nakajima, Y. Tamaki, K. Ueno, E. Kato, T. Nishikawa, K. Ohkubo, Y. Yamazaki, T. Morimoto and O. Ishitani, *J. Am. Chem. Soc.*, 2016, **138**, 13818–13821.
54 H. Koizumi, H. Chiba, A. Sugihara, M. Iwamura, K. Nozaki and O. Ishitani, *Chem. Sci.*, 2019, **10**, 3080–3088.
55 C.-Q. Jiao, Y.-S. Meng, Y. Yu, W.-J. Jiang, W. Wen, H. Oshio, Y. Luo, C.-Y. Duan and T. Liu, *Angew. Chem., Int. Ed.*, 2019, **58**, 17009–17015.
56 Q.-F. Gu, J.-H. He, D.-Y. Chen, H.-L. Dong, Y.-Y. Li, H. Li, Q.-F. Xu and J.-M. Lu, *Adv. Mater.*, 2015, **27**, 5968–5973.
57 P. Lang, R. Giereth, S. Tschierlei and M. Schwalbe, *Chem. Commun.*, 2019, **55**, 600–603.
58 H. Takeda, K. Koike, H. Inoue and O. Ishitani, *J. Am. Chem. Soc.*, 2008, **130**, 2023–2031.
59 M. L. Pegis, J. A. S. Roberts, D. J. Wasylenko, E. A. Mader, A. M. Appel and J. M. Mayer, *Inorg. Chem.*, 2015, **54**, 11883–11888.
60 I. Azcarate, C. Costentin, M. Robert and J. M. Saveant, *J. Am. Chem. Soc.*, 2016, **138**, 16639–16644.
61 E. S. Rountree, B. D. McCarthy, T. T. Eisenhart and J. L. Dempsey, *Inorg. Chem.*, 2014, **53**, 9983–10002.
62 M. L. Clark, P. L. Cheung, M. Lessio, E. A. Carter and C. P. Kubiak, *ACS Catal.*, 2018, **8**, 2021–2029.
63 A. Barthel, Y. Saih, M. Gimenez, J. D. A. Pelletier, F. E. Kühn, V. D'Elia and J.-M. Basset, *Green Chem.*, 2016, **18**, 3116–3123.
64 A. M. Chapman, C. Keyworth, M. R. Kember, A. J. J. Lennox and C. K. Williams, *ACS Catal.*, 2015, **5**, 1581–1588.
65 J. M. Smieja and C. P. Kubiak, *Inorg. Chem.*, 2010, **49**, 9283–9289.
66 X.-Q. Zhu, M.-T. Zhang, A. Yu, C.-H. Wang and J.-P. Cheng, *J. Am. Chem. Soc.*, 2008, **130**, 2501–2516.
67 H. J. Kuhn, S. E. Braslavsky and A. R. Schmidt, *Pure Appl. Chem.*, 2004, **76**, 2105–2146.